International Journal of Mass Spectrometry 279 (2009) 69–75

Contents lists available at ScienceDirect

International Journal of Mass Spectrometry

journal homepage: www.elsevier.com/locate/ijms

Dissociation of acetonitrile molecules following resonant core excitations

E. Kukk[a,*], R. Sankari[a], M. Huttula[b], S. Mattila[a], E. Itälä[a], A. Sankari[a,b], H. Aksela[b], S. Aksela[b]

[a] Department of Physics, University of Turku, FIN-20014 Turku, Finland
[b] Department of Physical Sciences, University of Oulu, Box 3000, FIN-90014 Oulu, Finland

ARTICLE INFO

Article history:
Received 26 June 2008
Received in revised form
12 September 2008
Accepted 19 September 2008
Available online 14 October 2008

Keywords:
PEPICO
Core excitation
Auger
Time-of-flight
Dissociation
Acetonitrile

ABSTRACT

Dissociation of acetonitrile molecules following resonant core excitations of carbon and nitrogen core electrons to the LUMO orbital was investigated using the electron-energy-resolved photoelectron–photoion coincidence (PEPICO) technique. The fragment ion mass spectra were recorded in coincidence with the resonant Auger electrons, emitted in the decay process of the core-excited states. Deuterated and ^{13}C-substituted samples were used for fragment identification. The results showed the initial core hole localization to be of minor importance in determining the dissociation pattern of the molecular cation. The participator and spectator Auger transitions produce entirely different fragmentation patterns and the latter indicates that complex nuclear rearrangements take place. Using also the findings from the ^{13}C labelling, it is suggested that the bending motion, induced in the core-excited state by the Renner–Teller effect, plays an important role in determining the most intense dissociation pathways of the spectator Auger final electronic states.

1. Introduction

Acetonitrile (C_2H_3N) is an organic molecule widely used in chemical industry as a solvent. Also known as methyl cyanide, it is the simplest of the organic nitriles. Acetonitrile molecule and a number of its fragments are also present in interstellar medium, where its dissociation is caused by cosmic rays. These molecules and ions play an important role in astrochemistry [1–3]. Dissociation of acetonitrile, both from gas phase and from adsorbed molecules, has been investigated by a number of experimental and theoretical studies [4–15]. It has become clear, that the dissociation process cannot be viewed simply as separation of the molecule into fragments, starting from its ground state geometry, along one or more broken bonds. Instead, nuclear rearrangements take place in the early stages of the dissociation. This process is related to the isomerization and therefore the dissociation and isomerization reactions should be considered together [8,11]. There are several known isomers of acetonitrile: in the neutral ground state the methyl cyanide configuration $CH_3–C{\equiv}N$ has the lowest energy, whereas the ionic state the ketenimine isomer $CH_2{=}C{=}NH$ is predicted to be the optimal configuration [11]. According to calculations, a number of other stable linear and cyclic geometries exist for the acetonitrile cation [8,16]. In the present work, the early stages of various dissociation pathways are discussed in terms of alternative isomerization reactions through theoretically predicted transition states.

Although the outcome of the dissociation reactions has been investigated using both electron [17,18] and photon [15] ionization as well as collision- or surface-induced ionization [7,11–14,16], little is known about how the dissociation depends on the nature of the intermediate short-lived excitation or on the electronic state of the parent molecular cation. Some earlier studies focused on electron–ion coincidences following nitrogen core excitations [9,10], but were lacking the electron energy measuring capability. On the other hand, Sekitani et al. [6] performed electron–ion coincidence (PEPICO) measurements on acetonitrile on gold surface with resolved electron energies and also scanning the photon energy across the core absorption structures, but they detected only the H^+ ions. Preliminary PEPICO results on the fragmentation of gas-phase acetonitrile were published in our instrumental paper [19].

When a photon of suitable energy is absorbed by molecule, electrons from core orbitals can be excited to the lowest unoccupied molecular orbital (LUMO). The resulting neutral core-excited state is energetically very unstable and decays by a resonant Auger process in a few femtoseconds, producing molecular cations. Depending on the fate of the LUMO electron, one can distinguish between the participator and spectator Auger decay. In the former, the LUMO electron is emitted and one valence hole created by filling the core hole; these resulting singly ionized electronic states

* Corresponding author.
E-mail address: edwin.kukk@utu.fi (E. Kukk).

1387-3806/$ – see front matter © 2008 Elsevier B.V. All rights reserved.
doi:10.1016/j.ijms.2008.09.015

are identical to those reached by direct valence photoionization. In the case of spectator Auger decay the photoexcited core electron remains in LUMO, one valence electron fills the core hole and another is emitted. The spectator Auger transitions to such states have a high probability, but in contrast these states can be only weakly populated (as satellite states) by direct valence photoionization. The presence of the excited electron in the antibonding LUMO orbital can have major consequences for the subsequent nuclear dynamics.

Using the pathway of resonant Auger decay to produce molecular cations thus opens access to a large variety of ionic electronic states which can be identified by the energy of the emitted Auger electron. In order to investigate the dependency of the molecular fragmentation on these states, the kinetic energy of the Auger electron must be recorded in coincidence with the ionic fragments. In this work, soft X-ray synchrotron radiation was used for the initial photoexcitation as its tunability allowed to selectively excite carbon or nitrogen core electrons. The end products were studied by ion mass (time-of-flight) spectroscopy in combination with electron spectroscopy using the electron–ion coincidence (PEPICO) technique.

A problem in PEPICO studies particularly for organic molecules is the unambiguous identification of the fragments based on their mass, since the PEPICO techniques employ rather simple linear ion TOF spectrometers which cannot resolve mass differences in the order of 1/1000th amu In order to resolve these ambiguities, isotopic substitutions – deuteration and isotopic labelling of the terminal carbon by ^{13}C – were used in the present work. The latter also allows us to identify, which carbon is contained in a fragment.

2. Experiment

As the experimental PEPICO setup has been described in detail in [19], a brief summary is given here. The setup consists of a modified Scienta SES-100 electron energy analyzer [20], where the original CCD camera was replaced by a resistive anode detector (Quantar), and a homemade Wiley-Mclaren type ion time-of-flight detector with a 400 mm long drift tube. The ion spectrometer is equipped by 77 mm Hamamatsu MCP detector with the anode consisting of 10 concentric rings. The ion TOF is determined by the recharge signal pulse from the MCP stack and the pulses from the anode rings are delayed by 50–100 ns with 5 ns steps. These can be used to determine the radial hit distance from the instrument's axis; in the present work the delayed pulse information was used in the data analysis stage to restrict the active area and improve the true/false coincidence ratio. The ion detection electronics is based on a 1 GHz waveform digitizer card (Signatec PDA 1000). The PEPICO system is operated in the pulsed extraction field mode and in the present experiment the extraction pulse voltage was 260 V across the sample region, with the drift tube held at −635 V.

The experiment was performed at beamline I411 at MAX-II synchrotron radiation facility (Lund, Sweden) [21]. Undulator radiation was monochromatized using a modified Zeiss SX-700 monochromator. The samples of acetonitrile, deuterated acetonitrile and isotopically substituted $^{13}CD_3$–C≡N were purchased from Sigma–Aldrich.

3. Results and discussion

3.1. Photoexcitation and resonant Auger decay

The photoabsorption spectrum of acetonitrile shows a prominent resonant structure below the N 1s ionization edge at $h\nu$ = 399.9 eV, assigned to the excitation of N 1s electron to LUMO

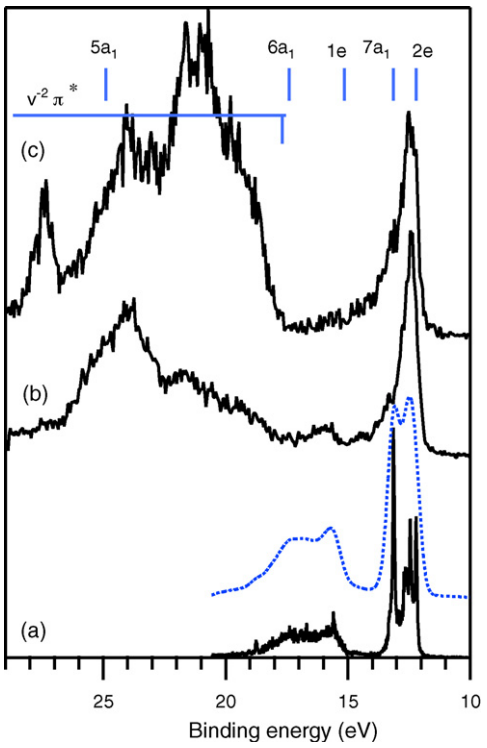

Fig. 1. Electron energy spectra for (a) nonresonant photoemission at $h\nu$ = 60.5 eV, dotted line-convoluted by 0.49 eV Gaussian, (b) resonant Auger decay after $C1s \rightarrow \pi^*$ excitations at $h\nu$ = 286.9 eV and (c) resonant Auger decay after $N1s \rightarrow \pi^*$ excitations at $h\nu$ = 399.9 eV. Orbital ionization energies and the range of the spectator Auger structures are marked.

[5,22] that has the π^* character along the C≡N bond in neutral acetonitrile (methyl cyanide isomer). Similar excitation feature is identified below the C 1s edge at 286.9 eV photon energy [5]. The $C1s \rightarrow \pi^*$ and $N1s \rightarrow \pi^*$ excitations were induced using 0.3 and 0.4 eV bandwidth (FWHM) monochromatized synchrotron radiation, respectively. Resonant Auger decay spectra of these excitations are shown in Fig. 1 together with a direct valence photoionization spectrum taken at $h\nu$ = 60.5 eV with 10 meV photon bandwidth. In order compensate for the differences in experimental resolution, Fig. 1(a) shows also the valence photoionization spectrum convoluted with a 0.49 eV FWHM Gaussian.

The Auger electron spectra at the C and N resonances exhibit a similar structure. The peak in the binding energy range from 12 to 14 eV corresponds to the participator transitions, populating the same single-hole states as in the nonresonant valence spectrum (a). The electronic states in this structure are, according to [24,25]:

E_b = 12.20 eV, $(2e)^{-1}$ – the valence orbital with mostly π_{CN} character,
E_b = 13.13 eV, $(7a_1)^{-1}$ – mostly N 2$p\sigma$,

The structure between 12 and 13 eV has been assigned to the vibrational progressions of the $(2e)^{-1}$ band. The vibrational progression is unresolved in the participator Auger spectra (b) and (c) and also the $(7a_1)^{-1}$ band shows much less resonant enhancement than the $(2e)^{-1}$ band. Next, the inner valence bands are visible in spectrum (a):

E_b = 15.13 eV, $(1e)^{-1}$ – pseudo π_{CH3} [25],
E_b = 17.4 eV – $(6a_1)^{-1}$ [26]

Transitions to these inner valence states are very weak in the resonant Auger spectra (b) and (c). The high binding energy region

above 18 eV covers two orbitals [26]:

$$E_b = 24.9\,\text{eV} - (5a_1)^{-1},$$
$$E_b = 29.7\,\text{eV} - (4a_1)^{-1} - \sigma_{CN}.$$

The resonant Auger spectra in this region show, instead, intense broad structures. The width of these structures indicates, that they originate mostly from spectrator Auger transitions covering a variety of two-hole, one-excited-electron combinations, studied in more detail by Gallet et al. [23]. We will refer to these states commonly as the $\nu^{-2}\pi^*$ states. Although the energy range is similar in the C and N decay spectra, the intensity distributions differ. In addition, there can be a contribution from the participator transitions to the $4a_1^{-1}$ and $5a_1^{-1}$ states, especially in spectrum (c).

3.2. Dissociation products

The ion TOF spectra of the molecular cations and ionic fragments following core excitation and resonant Auger decay were recorded using the PEPICO setup. The electron energy window was determined by the pass energy of the electron analyzer: the used 200 eV pass energy provided a 19 eV usable kinetic energy window, which was set to correspond to the binding energy range of Fig. 1. PEPICO data sets were recorded following both the $C1s \rightarrow \pi^*$ and $N1s \rightarrow \pi^*$ excitations. Ion TOF spectra were produced both from electron-triggered coincidence events and from randomly triggered events. Subtracting the latter from the electron-triggered events allowed us to remove the false coincidence background. The ion mass spectra shown in Fig. 2 have been converted from the TOF scale after background subtraction and represent only the true coincidences of ions with resonant Auger electrons. The fragment assignments are summarized in Table 1. The spectra (c) and (d) in Fig. 2 of the deuterated sample show some contamination peaks from the previously measured C_2H_3N sample that are marked by "x". This contamination of the gas inlet system could not be completely removed despite baking and pumping cycles between sample changes, it was likely caused by adsorbed acetonitrile on the surfaces of the gas inlet system, desorbing only when the next, deuterated acetonitrile sample was introduced. In order to take the contamination into account, first the percentage of the contamination molecules in the sample was determined using the $C_2ND_3^+/C_2NH_3^+$ parent molecular peak ratio. Then, for all peaks in spectra (c) and (d) the underlying undeuterated fragment intensities were calculated from their relative intensities in spectra (a) and (b), correspondingly, and subtracted.

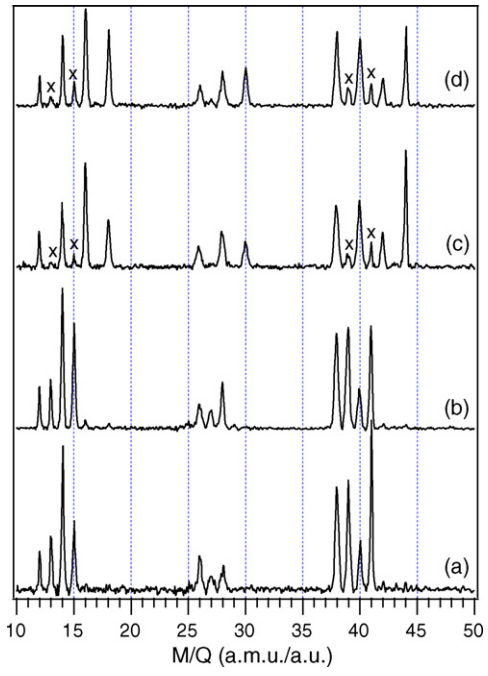

Fig. 2. Ion mass spectra measured in coincidence with resonant Auger electrons emitted from the decay of (a) $C1s^{-1}\pi^*$ at $h\nu = 286.9$ eV, C_2H_3N; (b) $N1s^{-1}\pi^*$ at $h\nu = 399.9$ eV, C_2H_3N; (c) $C1s^{-1}\pi^*$ at $h\nu = 286.9$ eV, C_2D_3N and (d) $N1s^{-1}\pi^*$ at $h\nu = 399.9$ eV, C_2D_3N.

Table 1
Fragmentation pattern of C_2H_3N and C_2D_3N molecules following $C1s \rightarrow \pi^*$ and $N1s \rightarrow \pi^*$ core excitations. *H* or *D* are commonly denoted by *X*. Masses of the deuterated fragments are given in brackets. Intensities are given in percent.

Fragment	Mass (amu)	$C1s \rightarrow \pi^*$	$N1s \rightarrow \pi^*$
C^+	12	3.1	2.9
CX^+	13(14)	5.8	4.5
CX_2^+	14(16)	15.3	15.4
CX_3^+	15(18)	7.6	11.7
N^+	14	0.0	0.0
NX^+	15(16)	0.6	0.7
NX_2^+	16(18)	0.7	1.1
NX_3^+	17(20)	0.0	0.0
C_2^+	24	0.0	0.0
C_2X^+	25(26)	0.7	1.4
$C_2X_2^+$	26(28)	4.2	3.5
$C_2X_3^+$	27(30)	0.4	1.2
CN^+	26	2.3	1.8
CNX^+	27(28)	3.1	2.3
CNX_2^+	28(30)	4.9	6.9
CNX_3^+	29(32)	0.0	0.0
C_2N^+	38	14.2	13.8
C_2NX^+	39(40)	14.0	15.0
$C_2NX_2^+$	40(42)	5.9	5.6
$C_2NX_3^+$	41(44)	15.8	11.1

In order to resolve mass ambiguities, PEPICO data from $CH_3–C{\equiv}N$, $CD_3–C{\equiv}N$ and $^{13}CD_3–C{\equiv}N$ samples were recorded. The ambiguous pairs in the mass spectrum of $CH_3–C{\equiv}N$ are: CH_2^+ and N^+ (M = 14 amu), CH_3^+ and NH^+ (M = 15 amu), $C_2H_2^+$ and CN^+ (M = 26 amu), $C_2H_3^+$ and HCN^+ (M = 27 amu). The fact that in the deuterated molecule the pairing is different was used for the identification of fragments, with the assumption that deuteration does not significantly alter the fragmentation pattern. The assumption is supported by the recent experiments on CH_4 and CD_4, where only slight differences in the fragmentation patterns were observed [27].

Relative weight factors were assigned to each of these fragments. The intensities of each mass peak were taken as sums of the fragment weight factors and the latter were optimized so that the best overall agreement with the experimental spectra of both the normal and deuterated sample was achieved. Least-squares minimization was used to obtain the best agreement. The results are summarized in Table 1. The table does not include the light H^+ and D^+ fragments. These peaks were observed in the mass spectrum, but since the detection efficiency of these fast fragments is small, quantitative intensity information is unreliable.

The analysis indicated that the N^+ fragments were not produced in our study, whereas Senba et al. deducted the presence of N^+ in their PEPICO spectra [9]. This discrepancy could be explained by the fact that since their study was not discriminating in electron energy, these ions could have been produced in coincidence with Auger electrons that have low kinetic energy (high binding energy, outside the range of our detection window). Electrons with such low kinetic energy correspond to the Auger final state energies above the double ionization threshold at $E_b = 33$ eV [28], where molecular dications are formed by secondary Auger decay prior to the dissociation. These dicationic dissociation mechanisms and products are completely different, with a number of ion–ion pairs produced.

Table 2
Terminal and central carbon in fragments in the ion mass spectra following the $C1s \rightarrow \pi^*$ excitation.

Mass	Common	Common %	C^t	C^c	C^t %
12				C^+	
13			C^+		50(20)
14	N^+	0		CD^+	
15			CD^+		64(15)
16	ND^+	4		CD_2^+	
17			CD_2^+		91(10)
18	ND_2^+	8		CD_3^+	
19			CD_3^+		90(15)
26				CN^+	
27	C_2D^+	23	CN^+		18(20)
28				CND^+	
29	$C_2D_2^+$	57	CND^+		29(10)
30				CND_2^+	
31	$C_2D_3^+$	8	CND_2^+		51(15)

In the present study, electron–ion–ion coincidences could also be extracted, but no such processes were observed since our binding energy window is below the double ionization threshold.

3.3. Terminal and central carbon in fragments

The above analysis does not identify, which of the two carbons belongs to a fragment. We will refer to the carbon in the methyl group as the terminal carbon C^t and in the cyano group as the central carbon C^c. In the third sample, C^t was labelled by the ^{13}C isotope and the molecule was deuterated: $^{13}C^tD_3–C^c{\equiv}N$. PEPICO datasets were recorded following the $C1s \rightarrow \pi^*$ and $N1s \rightarrow \pi^*$ excitations. Only fragments containing single carbon atoms are now of interest and are listed in Table 2. The comparison of the relevant regions in the mass spectra of the three samples is shown in Fig. 3. If a fragment contains only C^c, no shift occurs between spectrum (b) and (c), fragments containing only C^t are shifted by one mass unit and fragments containing either carbons are split in spectrum (c). In some cases, there are also "common" fragments that are not affected by the isotopic substitution (see Table 2). The fraction of the common fragment was calculated from the fragmentation pattern given in Table 1). Then, the probability for each fragment to contain C^t was

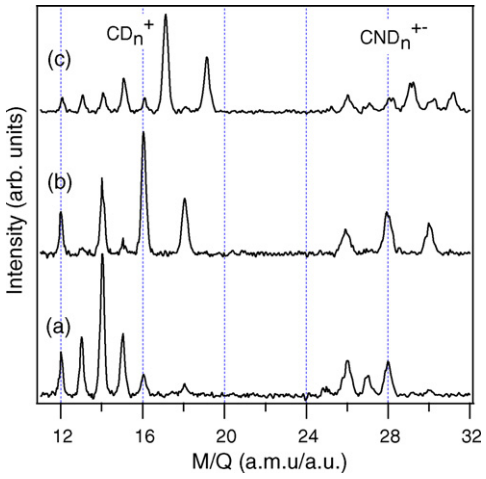

Fig. 3. Comparison of ion mass spectra recorded in coincidence with Auger electrons emitted in the decay of the $C1s^{-1}\pi^*$ resonance at $h\nu = 286.9$ eV. (a) $CH_3–C{\equiv}N$, (b) $CD_3–C{\equiv}N$ and (c) $^{13}CD_3–C{\equiv}N$. Labels indicate the main groups and peak masses are listed in Table 2.

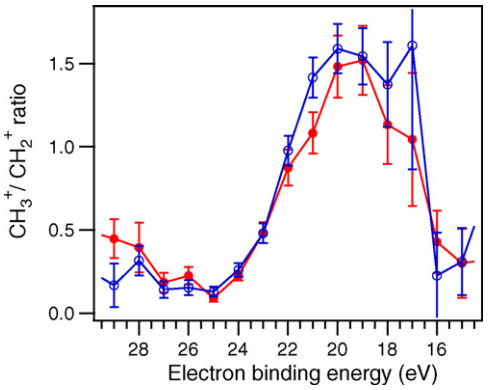

Fig. 4. Ratio of the CH_3^+ and CH_2^+ fragment ions as a function of coincident electron binding energy. (●) at $C1s^{-1}\pi^*$ resonance, (○) at $N1s^{-1}\pi^*$ resonance.

calculated from the peak intensities in spectrum (c), after correcting for the presence of the common fragment. The results are given in Table 2.

One can see that the methyl ion contains, within error limits, only C^t. This is expected, as simultaneous rebonding of all three D atoms to the central carbon seems highly unlikely and the ion is the result of the straightforward separation of the methyl group from the methyl cyanide isomer $C^tD_3–C^c{\equiv}N$. Also the CD_2^+ ion contains, within error bars, only the terminal carbon. It has been assumed to be a signature ion for the isomerization into the ketenimine form $C^tD_2{=}C^c{=}N\,D$ prior to the dissociation [13,7,11]. The ratio of CH_3^+ to CH_2^+ (which we have now confirmed to be $C^tH_3^+$ and $C^tH_2^+$) has been used to characterize the isotopic equilibrium of acetonitrile and ketenimine. Petris et al. argued, however, that this ratio from the ion mass spectra is very sensitive to the ionization conditions and is therefore poorly suited to describe this equilibrium [11]. The present study allows us to illustrate this point, by following the CH_3^+/CH_2^+ ratio as a function of the Auger final state energy (Fig. 4). These ions become abundant only in the spectrator Auger region above 17 eV binding energy, where one first observes a rapid increase of the CH_3^+/CH_2^+ ratio at both C and N 1s resonances, with a maximum at around 19–20 eV. The graph shows that the ratio is indeed very sensitive to the conditions of creating the molecular cation, although it is not clear, whether the dependency is due to different cationic electronic states being populated, or from changes in the internal energy of the parent cation.

The situation is quite different for the lightest fragments. Firstly, about 1/3 of the CD^+ ions contain the central carbon. As an explanation, one can look at theoretically modelled isomerization reactions of the methyl cyanide cation [8]. One pathway leads to the formation of the ketenimine ($C^tD_2{=}N{=}C^cD$) geometry, in which case the separation of C^cD^+ fragment could be regarded as an "overshoot" in the creation of the C^cD group. In a more detailed look into nuclear dynamics, Petris et al. [11] and Choe et al. [8], predicted isomerization into the ketenimine form to proceed over a cyclic transition state with a CCN triangle and a H (or D) atom bonded to each of them. This geometry can be particularly relevant in explaining the second experimental finding, the equal probability of the C^+ fragment of being C^c or C^t (Table 2), since both carbons are equivalent in the triangular transient geometry.

In contrast to the CH_n^+ ions, the CN^+ fragment contains mostly the central carbon atom, indicating again the possibility of a straightforward separation of the cyano group from methyl cyanide. Also the CND^+ contains mostly the central carbon, which can be interpreted as the separation of this group from the ketenimine geometry $C^tD_2–C^c{=}ND$. Perhaps the most interesting is the equal presence of the terminal and central carbons in the CND_2^+ frag-

ment. Here, one again notices the cyclic transition state geometry in the sequence of isomerization, predicted by theory. Breaking the *C–N* and *C=C* bonds in the *CCN* triangle would yield the $C^cD_2^+$ and the $C^tD_2^+$ fragments with equal probability.

3.4. Electronic state dependent dissociation

In the previous analysis, the energy of the Auger electrons was determined only with the 19-eV width of the detector energy window, although during the PEPICO measurement the accurate electron energy was recorded for each event by the position sensitive detector. Next, the energy dependency of the ion production is investigated. Fig. 5 displays the electron–ion coincidence map for the $C1s^{-1}\pi^*$ Auger decay, with electron binding energy as x-axis and ion TOF as *y*-axis. The map was produced by histogramming all PEPICO events and subtracting the false coincidence events. The 2*D* histogram was smoothed slightly to improve readability. Fig. 6 displays the analogous map recorded in coincidence with the electrons from the $N1s^{-1}\pi^*$ Auger decay.

Both PEPICO maps show a very similar structure, which leads to the conclusion that, in the present case, the atomic site of initial core excitation is not an important factor determining the dissociation pathways. The participator decay to the $2e^{-1}$ states at 12 eV does not lead to dissociation and predominantly the parent molecular cation $C_2NH_3^+$ is observed. At the high-energy shoulder of this peak in the electron spectrum, neutral hydrogen loss starts to occur, as the intensity of the $C_2NH_n^+$, $n=0$–2 fragments increases. The change can be attributed to the changing electronic character, as the $7a_1^{-1}$ states start to be populated. However, it can also be due to the increase of the excess energy in the molecule, as the Auger decay reaches the higher-energy regions of the $2e^{-1}$ potential energy surface with the increasing binding energy. As our recent PEPICO study of CH_4 showed, both mechanisms were relevant in explaining the electron-energy-dependency of molecular fragmentation [27]. The barrier height of the local potential energy minimum for the methyl

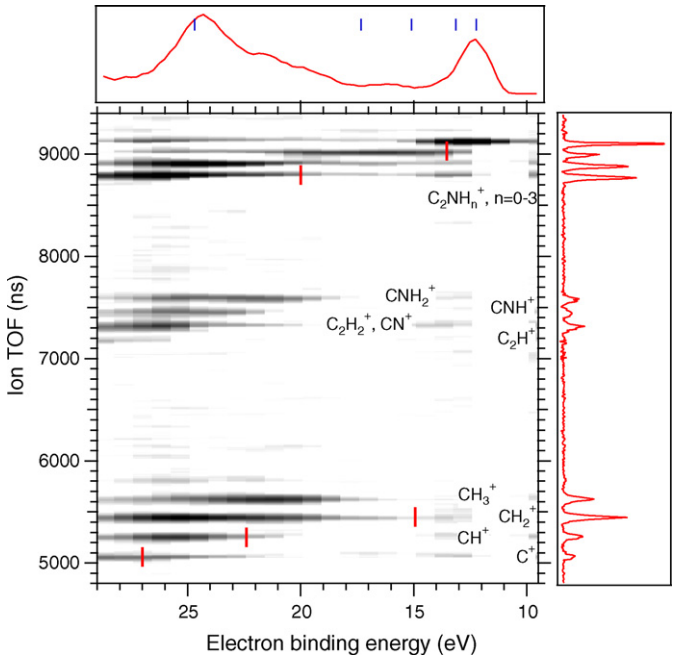

Fig. 5. Electron–ion coincidence (PEPICO) map of C_2H_3N from the Auger decay of the $C1s^{-1}\pi^*$ resonance at $h\nu = 286.9$ eV. The top panel shows the electron energy spectrum and the right-hand panel the ion TOF spectrum, both integrated from the data in the PEPICO map.

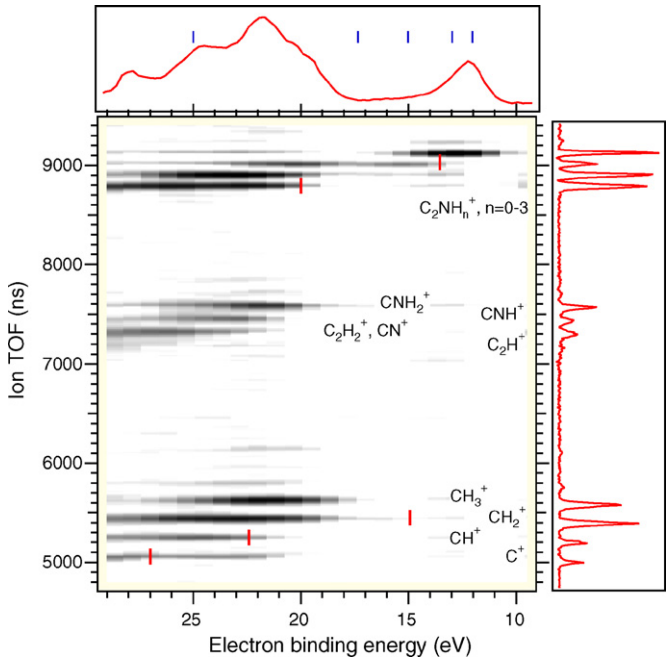

Fig. 6. PEPICO map of C_2H_3N from the Auger decay of the $N1s^{-1}\pi^*$ resonance at $h\nu = 399.9$ eV. The top panel shows the electron energy spectrum and the right-hand panel the ion TOF spectrum.

cyanide isomer of the cation is about 0.7 eV [11], which predicts a sudden increase in the probability of molecular dissociation at around 12.9 eV electron binding energy in the PEPICO maps (first ionization potential + the barrier height). This is indeed in accordance with the experiment.

The region of the $(1e)^{-1}$ ($E_b = 15.1$ eV) and $(6a_1)^{-1}$ ($E_b = 17.4$ eV) states is dominated by the fragment with a single hydrogen loss, $C_2N\,H_2^+$ As the cation is now created not in its lowest electronic state, the available internal energy (while remaining on that potential energy surface) is smaller. This region around 14–18 eV binding energy corresponds best to the case of the ionized molecule having sufficient energy to isomerize into ketenimine, but losing the hydrogen atom that is migrating from the methyl to the cyano group.

Then, at around 18 eV, the onset of the spectator region with the transitions to the $v^{-2}\pi^*$ states shows a major change in the dissociation pattern. The parent cation almost disappears from the ion mass spectrum and the fragments CH_n^+, $n=0$–3, C_2H^+, $C_2H_2^+$ and CN^+ are produced instead. We particularly note the strong presence of the ethyne (acetylene, $C_2H_2^+$) and hydrogen cyanide (HCN^+) cations and protonated hydrogen cyanide (H_2CN^+). These ions have been observed in interstellar matter and have been assigned an important role in astrochemistry. A closer observation of the PEPICO maps shows that the dissociation patterns changes also within the spectator structure, e.g., the $C_2H_2^+$, CN^+ and C_2H^+ ions become abundant only above ≈22 eV electron binding energy.

The third PEPICO map (Fig. 7) is constructed from the coincidence events following the $C1s^{-1}\pi^*$ Auger decay in the ^{13}C labelled sample. The region displayed corresponds to the ions, where the distinction between the terminal and central carbon can be made and also shows only the electron energy range of spectator Auger transitions, since participator transitions do not produce these ions. The electron-energy-independent analysis of these fragments was summarized in Table 2, but from the PEPICO map one can investigate, whether the C^t/C^c ratio is electronic state dependent. As seen from Fig. 7, there is no clear evidence for any such dependency. For the $C\,N\,D^+$ fragments, probability for the fragment to contain C^t

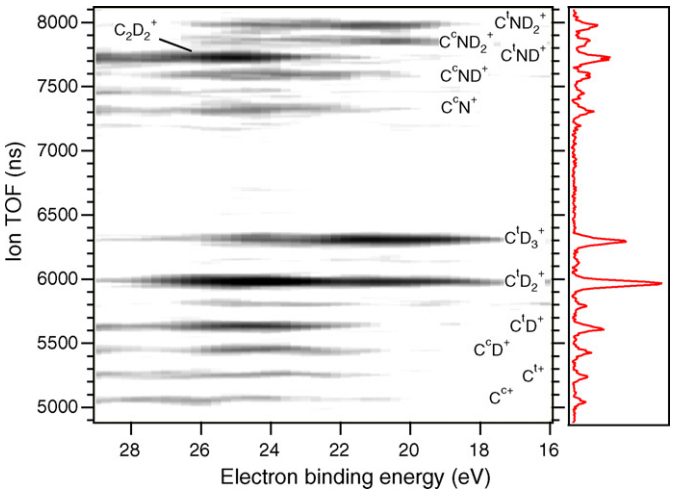

Fig. 7. PEPICO map from Auger decay of the $^{13}C\ D_3–C{\equiv}N$ sample from the Auger decay at $C1s^{-1}\pi^*$ resonance. The right-hand panel shows the ion TOF spectrum.

instead of C^c seems to be higher at higher electron binding energies, but the strong presence of the $C_2D_2^+$ ion obscures this comparison.

3.5. Influence of nuclear dynamics in core-excited states

The drastic changes in the PEPICO maps when going from single-hole states to the $\nu^{-2}\pi^*$ states suggests that the presence of an electron in the antibonding LUMO orbital has major consequences. Its influence can be qualitatively predicted from the behaviour of the molecule already in the core-excited state, since changes in the molecular geometry begin immediately after the core excitation.

Carniato et al. [22] have analyzed the nuclear dynamics in the $N1s^{-1}\pi^*$ state. Promotion of an electron to the LUMO orbital does not, in itself, create a dissociative state. LUMO is in the ground as well as excited state, a π^*_{CN} type orbital, with some electron density also around the H atoms. The core-excited state undergoes a Renner–Teller splitting, removing the degeneracy of the LUMO orbital by bending the initially linear $C–C{\equiv}N$ group. The new equilibrium (about 1.1 eV lower) is obtained at the $C–C{\equiv}N$ angle of about 130°. The geometry change induces excitations of high harmonics (n = 15–17) of the relevant bending vibrational mode with the oscillation of the $C–C{\equiv}N$ angle between 0° and 100°. However, the core-hole lifetime (<10 fs) is considerably shorter than the vibrational period (71 fs) of the $C–C$ bending mode and thus the molecule after Auger decay will be at an early stage of bending the $C–C{\equiv}N$ chain out of linear geometry. This is the initial motion of the dissociating cation following core excitation, and it is lacking in a molecular cation produced by direct valence photoionization.

In the participator Auger decay the LUMO electron is removed, therefore removing also the bending force, whereas in spectator Auger, the presence of the electron in LUMO continues to bend the molecular cation. One can speculate that this motion is a key factor in explaining the differences on how the dissociation will proceed in direct valence ionization, after participator Auger and after spectator Auger decay. The first two display very similar dissociation patterns, indicating that the geometry change in the core-excited state has not had a significant impact and the presence of the LUMO electron is needed also in the cationic state in order to influence the dissociation. For example, as noted earlier, 50% of the C^+ fragments were the central carbon atoms, that can be explained by the existence of a triangular transition state [8,11,16]. The strong bending excitation facilitates the formation of the triangluar form, which suggests that the cyclic transition-state geometry is relevant when modelling the dissociation of the spectator Auger final states. It is also notable that the C^+ fragments in the PEPICO maps of Fig. 5 and especially in Fig. 6 appear about 6 eV below the ion appearance threshold energy of 27 eV [29]. This supports the hypothesis that the bending motion induced in the core-excited state helps to cross the barrier into this fragmentation channel.

The significance of the bending nuclear motion induced in the core-excited state by the Renner–Teller splitting in determining the branching ratios of the molecular dissociation has been observed earlier in the CO_2 molecule by Morin et al. [30]. In that case it was also observed that fine tuning the photon energy to map different portions of the core-excited Renner–Teller split states alters the dissociation pattern. In future studies, it would be of interest to study such dependencies also in acetonitrile, thus clarifying the role of the bending vibrational excitations.

The second effect of the core-excited state on the molecular dissociation is related to the localization of the core hole to a specific atom. Liu et al. observed major differences in fragment production following resonant excitations of C 1s or F 1s electrons in the CH_3F molecule [31]. In contrast, the differences between the fragment yields following carbon or nitrogen core excitations are minor in the present work (see Table 1). In the case of CH_3F, the strong core-hole localization dependency was explained in terms of ultrafast dissociation, which starts as the elongation of the $C–F$ bond already in the core-excited state and thus leaves the core hole localized on either side of the breaking bond. The Auger decay and the creation of an ion then take place in an essentially fragmented molecule. In the case of C_2H_3N, the core-excitation induced motion is bending of the CCN chain and, as proposed above, it leads to a cyclic transition state geometry rather than to ultrafast dissociation. Therefore, the Auger decay still takes place in nonfragmented parent ion and the "memory" of core hole localization is lost before fragmentation.

4. Conclusions

We have investigated the dissociation of the acetonitrile molecule following both carbon and nitrogen resonant core excitations to the LUMO orbital. The fragmentation pattern showed little dependency on the initial site of core hole creation, attributed to the bonding nature of the core-excited state. On the other hand, the PEPICO maps revealed major changes in the fragmentation patterns depending on the final cationic state reached by Auger decay of the core-excited states. In particular, the spectator Auger region shows that much more complex dissociation pathways are involved than in the case of single valence hole states reached by participator Auger or direct ionization. We suggest that the major influencing factor is the bending of the $C–C{\equiv}N$ linear chain that is initiated already in the core-excited state due to the Renner–Teller splitting. The appearance of different ionic fragments was also related to the several known isomers of $C_2H_3N^+$ and it was shown that whereas some fragments such as CH_3^+ or NH^+ can be interpreted as separating from the methyl cyanide or ketenimine isomers, for a number of others the production pathway is less straightforward.

The origin of different fragments was further clarified using the sample with isotopically substituted terminal carbon and it was found that the C^+ and $C\ N\ D_2^+$ fragments contain the central and terminal carbon in equal proportion and that the central carbon contributed significantly also to the CD^+ ions. These findings have no direct bearing to the straightforward separation reactions of the common methyl cyanide and ketenimine forms; instead their appearance can be relevant to the bending distortion of the molecule and the existence of a cyclic, triangular geometry of a transition state in isomerization reactions. In general, the present study confirmed the very sensitivity of the molecular dissociation on the electronic transitions leading to the formation of the parent

cation, which calls for caution in deriving, for example, the isomeric constitution of the parent cations from the ratios of certain ionic fragments in the mass spectrum.

Acknowledgements

This work was supported by EC "Access to Research Infrastructure" programme. Financial support by the Academy of Finland is acknowledged. The authors thank the staff of MAX-lab for their help during the experiments and Profs. E. Rachlew and M. Stankiewicz for their contribution to the TOF instrumentation.

References

[1] R.L. Hudson, M.H. Moore, Icarus 172 (2004) 466.
[2] V. Ngassam, A.E. Orel, A. Suzor-Weiner, J. Phys.: Conference Series 4 (2005) 224.
[3] H. Tachikawa, Phys. Chem. Chem. Phys. 1 (1999) 4925.
[4] D.M. Rider, G.W. Ray, E.J. Darland, G.E. Leroi, J. Chem. Phys. 74 (1981) 1652.
[5] Ph. Parent, C. Laffon, F. Bournel, J. Chem. Phys. 112 (2000) 986.
[6] T. Sekitani, E. Ikenaga, K. Tanaka, K. Mase, M. Nagasono, S. Tanaka, T. Urisu, Surface Sci. 390 (1997) 107.
[7] C. Mair, Z. Herman, J. Fedor, M. Lezius, T.D. Mark, J. Chem. Phys. 118 (2003) 1479.
[8] J.C. Choe, Int. J. Mass Spectrom. Ion Process. 235 (2004) 15.
[9] Y. Senba, H. Yoshida, T. Ogata, D. Sakata, A. Hiraya, K. Tanaka, J. Electron Spectrosc. Relat. Phenomena 101–103 (1999) 131.
[10] C. Harada, S. Tada, K. Yamamoto, Y. Senba, H. Yoshida, A. Hiraya, S. Wada, K. Tanaka, K. Tabayashi, Rad. Phys. Chem. 75 (2006) 2085.
[11] G. de Petris, S. Fornarini, M.E. Crestoni, A. Troiani, P.M. Mayer, J. Phys. Chem. A 109 (2005) 4425.
[12] J. van Thuijl, J.J. van Houte, A. Maquestiau, R. Flammang, C. DeMeyer, Org. Mass Spectrom. 12 (1977) 196.
[13] E.K. Chess, R.L. Lapp, M.L. Gross, Org. Mass Spectrom. 17 (1982) 475.
[14] J.L. Holmes, P.M. Mayer, J. Phys. Chem. 99 (1995) 1366.
[15] E. Ruhl, S.D. Price, L. Leach, J.H.D. Eland, Int. J. Mass Spectrom. Ion Process. 97 (1990) 175.
[16] E. Marotta, P. Traldi, Rapid Commun. Mass Spectrom. 17 (2003) 2846.
[17] W. Heerma, J.J. de Ridder, D. Dijkstra, Org. Mass Spectrom. 2 (1969) 1103.
[18] P.W. Harland, B.J. McIntosh, Int. J. Mass Spectrom. Ion Process. 69 (1985) 29.
[19] E. Kukk, R. Sankari, M. Huttula, A. Sankari, H. Aksela, S. Aksela, J. Electron Spectrosc. Relat. Phenomena 155 (2007) 141.
[20] M. Huttula, S. Heinasmaki, H. Aksela, E. Kukk, S. Aksela, J. Electron Spectrosc. Relat. Phenomena 156–158 (2007) 270.
[21] M. Bassler, A. Ausmees, M. Jurvansuu, R. Feifel, J.-O. Forsell, P. de Tarso Fonseca, A. Kivimaki, S. Sundin, S.L. Sorensen, R. Nyholm, O. Bjorneholm, S. Aksela, S. Svensson, Nucl. Instrum. Methods Phys. A 469 (2001) 382.
[22] S. Carniato, E. Kukk, J.-J. Gallett, B. Brena, Y. Luo, Phys. Rev. A 71 (2005) 22511.
[23] J.-J. Gallet, F. Bournel, S. Kubsky, G. Dufour, F. Rochet, F. Sirotti, J. Electron Spectrosc. Relat. Phenomena 122 (2002) 285.
[24] D.C. Frost, F.G. Herring, C.A. McDowell, I.A. Stenhouse, Chem. Phys. Lett. 4 (1970) 533.
[25] M. Gochel-Dupuis, J. Delwiche, M.-J. Hubin-Franskin, J.E. Collin, Chem. Phys. Lett. 193 (1992) 41.
[26] L. Asbrink, W. von Niessen, G. Bieri, J. Electron Spectrosc. Relat. Phenomena 21 (1980) 93.
[27] E. Kukk, G. Pruemper, R. Sankari, M. Hoshino, C. Makochekanwa, M. Kitajima, H. Tanaka, H. Yoshida, Y. Tamenori, E. Rachlew, K. Ueda, J. Phys. B 40 (2007) 3677.
[28] A. Bayliss, S.E. Silcocks, F.M. Harris, S. R: Andrews, D.E. Parry, Int. J. Mass Spectrom. Ion Process. 163 (1997) 121.
[29] S.G. Lias, J.E. Bartmess, J.F. Liebman, J.L. Holmes, R.D. Levin, W.G. Mallard, Ion energetics data, in: P.J. Linstrom, W.G. Mallard (Eds.), NIST Chemistry WebBook, NIST Standard Reference Database Number 69, June 2005. Available from: <http://webbook.nist.gov>.
[30] P. Morin, M. Simon, C. Miron, N. Leclercq, E. Kukk, J.D. Bozek, N. Berrah, Phys. Rev. A 61 (2000) 050701.
[31] X.-J. Liu, G. Prumper, E. Kukk, R. Sankari, M. Hoshino, C. Makochekanwa, M. Kitajima, H. Tanaka, H. Yoshida, Y. Tamenori, K. Ueda, Phys. Rev. A 72 (2005) 042704.